CHEMISTRY OF MATERIALS

pubs.acs.org/cm

Methods/Protocols

Guidelines for Synthesis and Processing of Chemically Stable Two-Dimensional V_2CT_x MXene

Kyle Matthews, Teng Zhang, Christopher E. Shuck, Armin VahidMohammadi, and Yury Gogotsi*

Cite This: *Chem. Mater.* 2022, 34, 499−509

Read Online

ACCESS | Metrics & More | Article Recommendations | Supporting Information

ABSTRACT: Vanadium carbide MXenes, specifically V_2CT_x, have shown promise for applications ranging from energy storage and sensing to electronics and optics. In the past decade, however, research involving V_2CT_x has been mostly limited to its multilayered form due to instability of delaminated V_2CT_x in its colloidal state. In this paper, we report on mild synthesis conditions which result in high-quality V_2CT_x and an ion exchange process coupled with flocculation that increases the shelf life of this MXene in aqueous suspension by about 3 orders of magnitude, from a few hours to several months. We discuss the etching and delamination mechanisms and provide a guideline for researchers working with this MXene composition. We explain the effect of etchant formulation, delamination chemicals, and postprocessing on the quality, chemical stability, and optoelectronic properties of the synthesized V_2CT_x. We also demonstrate that during ion-exchange and flocculation tetrabutylammonium or tetramethylammonium ions are replaced with lithium cations. The produced precipitates from delaminated V_2CT_x can not only be stored in suspension for a few months without degradation but can also be redispersed and processed into films. Those MXene films show distinct improvements in the optical and electronic properties. Their electrical conductivities in the dry state can exceed 1000 S cm^{-1}, a value not previously achievable for V_2CT_x. The major improvements in shelf life and properties of V_2CT_x demonstrated in this work are expected to allow fundamental studies of properties of this MXene and greatly expand its range of potential applications. The proposed approach may be applicable to other MXenes that require the use of quaternary amines for delamination.

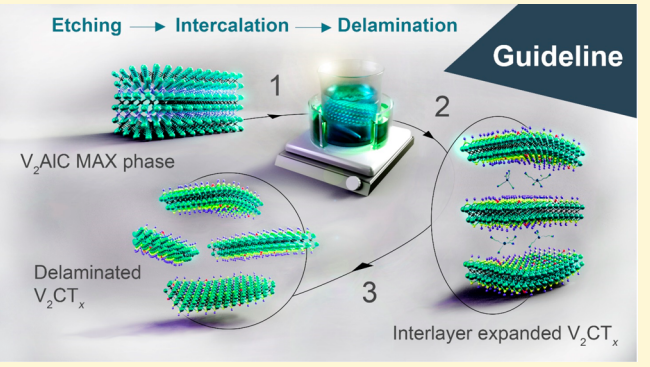

INTRODUCTION

Since their discovery in 2011,[1] two-dimensional (2D) transition metal carbides and nitrides, MXenes, have shown promising electrical,[2] mechanical,[3] optical,[4] and electrochemical properties leading to their widespread use in applications such as energy storage,[5] electromagnetic interference shielding,[6,7] sensing,[8,9] electronics,[10,11] and biomedicine,[12−14] to name a few. MXenes have a general formula of $M_{n+1}X_nT_x$, where M represents early transition metals (Ti, V, Nb, etc.), X is carbon and/or nitrogen, n = 1−4, and T_x represents the surface functional groups (−O, −OH, −F, −Cl) on these materials.[15] The possibility of having a single transition metal or different multiple transition metals, in an ordered or solid solution (random) form, on the M site along with C and/or N in the X site, has resulted in the experimental synthesis of more than 30 stoichiometric MXene compositions with many more computationally predicted.[16] However, despite the numerous MXene compositions available, research has primarily focused on $Ti_3C_2T_x$, mainly because of its high chemical stability and the presence of established synthesis guidelines.

Among other MXenes, the M_2XT_x structure, in particular V_2CT_x, is interesting due to its larger active area per mass (lower number of atomic layers in their structure; three atomic layers for V_2C vs five atomic layers for Ti_3C_2) with a more chemically active transition metal (vanadium) that has multiple oxidation states. Multilayer (*ml*-V_2CT_x) or delaminated films of V_2CT_x (*d*-V_2CT_x) have been used in various applications such as batteries,[17,18] supercapacitors,[19] gas sensors,[20] electronics,[21] optics,[22] and biomedicine.[14] Similar to other MXenes, density functional theory calculations (DFT) have suggested that bare and F/OH terminated V_2C should show metallic behavior;[23] however, because of the presence of large organic intercalants (used for delamination) in the interlayer space of V_2CT_x flakes, experimental measurements have shown semiconductor-like electronic behavior and a negative temperature-dependent resistivity change for V_2CT_x multilayer films.[24] The unusual electronic properties of *d*-V_2CT_x have

Received: October 9, 2021
Revised: December 13, 2021
Published: December 29, 2021

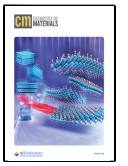

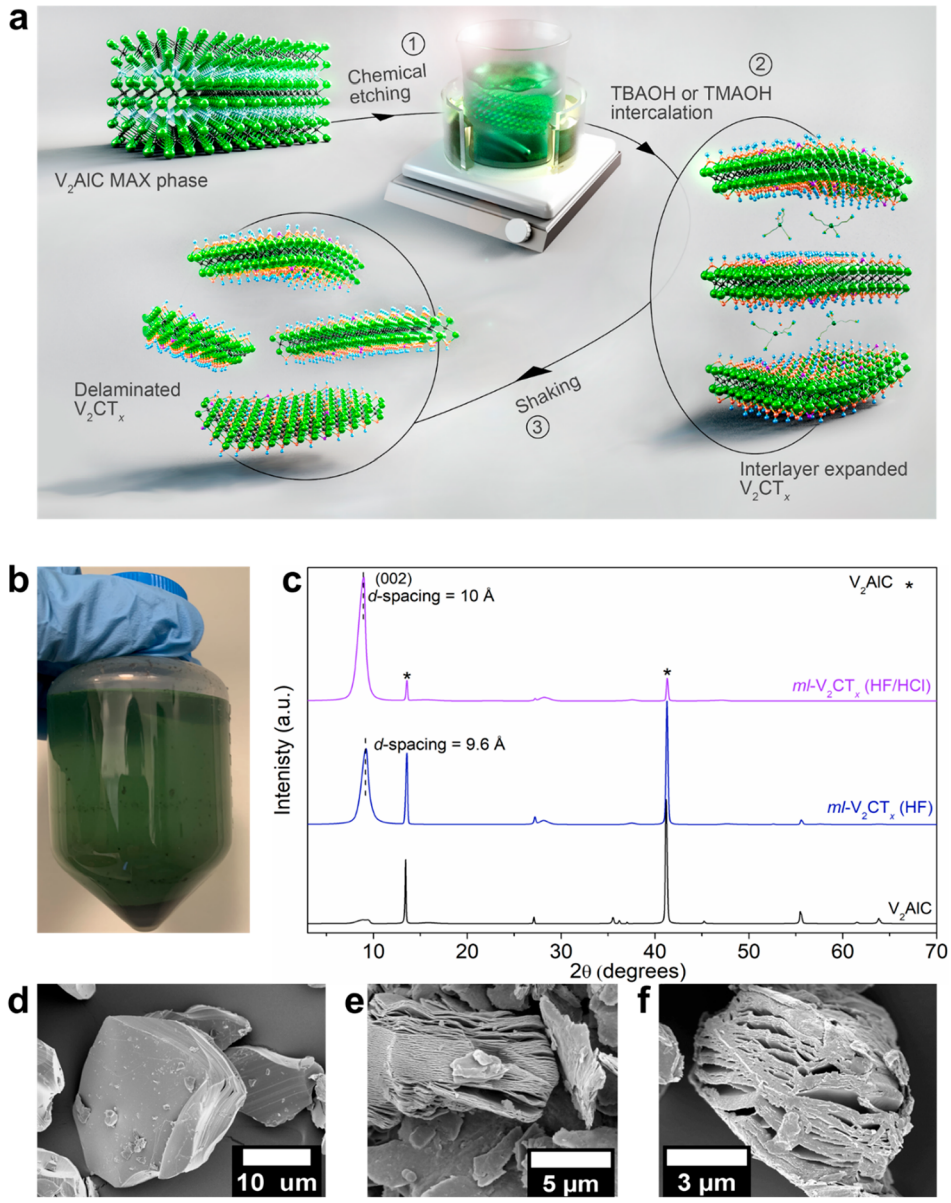

Figure 1. (a) Schematic of MXene synthesis process. (b) XRD patterns of V_2AlC MAX and multilayer V_2CT_x made by HF etching and mixed acid synthesis methods. (c) Optical image of first supernatant (green) after washing. SEM images of the (d) V_2AlC MAX phase, (e) multilayer V_2CT_x from HF etching, and (f) multilayer V_2CT_x from mixed acid etching.

rendered it promising for various optoelectronic applications. For example, transparent conductive electrodes made from spin-coated thin films of V_2CT_x have shown a higher figure of merit (FOM) compared to those of other M_2XT_x MXenes, such as Ti_2CT_x.[21]

Despite this promise, V_2CT_x is anecdotally known to be the least chemically stable MXene in its delaminated form. Single and few-layer V_2CT_x flakes readily degrade in water dispersions or when exposed to air. Because of this instability, previous studies have mostly focused on *ml*-V_2CT_x rather than *d*-V_2CT_x.[25] In addition, V_2CT_x is commonly delaminated by large organic molecules such as tetramethylammonium hydroxide (TMAOH) or tetrabutylammonium hydroxide (TBAOH). Since complete removal of TBA^+ or TMA^+ ions is difficult to achieve, produced V_2CT_x films usually show a large interlayer spacing. This, along with the highly defective nature of V_2CT_x flakes[17,19] as well as its other intrinsic properties, have so far resulted in lower electrical conductivities (140 S cm^{-1}) compared to $Ti_3C_2T_x$.[21,26,27]

To overcome the chemical instability of V_2CT_x (and other less stable MXenes, such as Ti_2CT_x), numerous post-processing approaches including the addition of polyanionic salts to hinder edge-driven oxidation, adjustment of the colloidal solution pH with buffers, and antioxidants have been used.[28,29] While these approaches lead to improved MXene chemical stability in water dispersions, they negatively affect the electronic and electrochemical properties. Using buffers in solution, whether acidic or basic, decreases the electrical conductivity of vacuum filtered films. Moreover, the use of alkaline buffers led to faster MXene degradation over time.[29] In addition to postprocessing treatments, the quality of the MAX phase precursor and initial etching and delamination

https://doi.org/10.1021/acs.chemmater.1c03508
Chem. Mater. 2022, 34, 499−509

conditions are also important factors for the synthesis of higher quality and chemically stable V_2CT_x flakes, which has already been shown for $Ti_3C_2T_x$.[27,30] Therefore, to practically use V_2CT_x for research or device applications, after confirming proper stoichiometry and particle size of the V_2AlC MAX phase precursor, first, the etching and delamination conditions should be improved to produce higher quality V_2CT_x flakes. Second, proper protocols should be developed to improve its chemical stability without negatively affecting its properties. The combination of these two improvements will alleviate existing challenges facing the community, enabling more widespread use of V_2CT_x.

In this guideline, we discuss the improved etching and delamination protocols for the synthesis of V_2CT_x and show that, through an ion exchange approach coupled with flocculation, *d*-V_2CT_x flakes can be stored for several months with no significant degradation occurring even after ∼150 days. We use a mixed acid etchant formulation to synthesize *ml*-V_2CT_x, followed by delamination with TBAOH or TMAOH. A LiCl ion-exchange/flocculation process is used as a postprocessing technique to stabilize the *d*-V_2CT_x flakes. This approach both improves its chemical stability and nearly doubles the electrical conductivity of V_2CT_x freestanding films. We attribute these enhancements to the replacement of the TBA^+ or TMA^+ with Li^+ ions, indicated by a significant reduction in the *d*-spacing of the MXene films and their increased conductivity above 1000 S cm^{-1}.

DISCUSSION OF METHODS

Precursor and Etching Conditions. Research on $Ti_3C_2T_x$ has shown that properties and morphology of the prepared MXene depend on the stoichiometry, quality, and particle size of the MAX phase precursor.[15] For example, it was recently shown that increasing the Ti_3AlC_2 MAX phase quality by controlling its stoichiometry leads to less defective $Ti_3C_2T_x$ flakes with enhanced chemical stability.[30] Similarly, the successful synthesis of high quality V_2CT_x depends on the stoichiometry and quality of the V_2AlC MAX phase precursor. For the synthesis of V_2AlC, vanadium (99.5%, −325 mesh), aluminum (99.5%, −325 mesh), and graphite (99%, −325 mesh) powders are used. First, V, Al, and C precursors are mixed in a 2:1.1:0.9 atomic ratio (e.g., 50 g total per batch). The precursors are ball-milled with 10 mm yttria stabilized zirconia balls (2:1 ball:powder mass ratio) in plastic jars at 60 rpm for 18 h to ensure a homogeneous mixture of the powders. The powder mixture is transferred into alumina crucibles and placed into a high-temperature tube furnace (Carbolite Gero). The furnace should be purged with ultrahigh purity Ar gas (200 SCCM) prior to heating for at least 1 h. Argon should also be continually flown through the furnace throughout the sintering procedure. The furnace is heated to 1550 °C at a rate of 3 °C min^{-1}, held for 2 h, and then cooled to room temperature at a rate of 3 °C min^{-1}. Afterward, the sintered compact can be milled using a TiN-coated bit or crushed with a mortar and pestle and then sieved to the desired particle size (usually <38 μm (400 mesh)). The sieving process ensures a uniform particle size distribution and similar etching kinetics between the MAX particles. The obtained V_2AlC particles usually contain unreacted elemental powders or intermetallic impurities. They can be removed by acid washing the MAX powders in 9 M HCl for 12 h. A total of 2 mL of 9 M HCl was used for every gram of V_2AlC. Afterward, the V_2AlC particles are washed by filtration with deionized water until a pH of >5−5.5 is achieved.

Figure 1a schematically shows different steps involved for the synthesis of V_2CT_x. Typically, V_2AlC is etched in 48−50% hydrofluoric acid (HF). So far, efforts to use acid and alkali salt mixture etchants have not been successful. HF is a harsh etchant and results in defective/low quality MXene multilayers and flakes.[31] In order to overcome damage from concentrated HF, we developed a milder etchant based on a mixture of HF and hydrochloric acid (HCl) for the synthesis of V_2CT_x, the details of which are provided in the following text. Etching should be done in high density polyethylene (HDPE) bottles, and per 1 g of V_2AlC, 20 mL of etching solution (either pure HF or HF/HCl as described below) is required. To ensure safety and proper mixing, the etching bottle should be selected so that the etchant does not occupy more than one-third of its volume. For example, 1 g of V_2AlC can be etched in a 60 mL HDPE bottle, but if 2 g of V_2AlC powder is required to be etched, the volume of etchant solution will be 40 mL; therefore, a larger HDPE bottle (i.e., 125 mL) should be used. Moreover, it is important to use an ice bath for the addition of V_2AlC because the highly reactive particles can experience local heating (as the result of exothermic reactions between MAX phase powder and the acidic etchant), which can cause instant oxidation/dissolution. Therefore, after placing the etchant bottle in an ice bath (Figure S2a), slowly, 1 g of V_2AlC is added to the etchant while stirring the solution at low speed (150 rpm). The addition of powder should usually take ∼5 min per gram of MAX phase. After all the powder is added, it is suggested to monitor the reaction for 1−2 min to make sure no severe reaction is occurring (no bubbling should be observed). Then the bottle is loosely capped and subsequently transferred to an oil bath to start the etching in a controlled temperature condition as described below. The stirring speed can be fixed at 400 rpm for all etching conditions. The proper safety precautions must be carried out when working with HF, as recently outlined.[32]

We investigated the effect of the etching time of V_2AlC in HF and HF/HCl solutions and determined the minimal time required for the most complete conversion of V_2AlC into V_2CT_x without inherent oxidation. The table in Figure S1 outlines the different etching configurations tested. The premise of a mixed acid etch was based on previous work with $Ti_3C_2T_x$.[33] For the conventional HF etching protocol, 20 mL of 48 wt % HF is used per 1 g of MAX phase, and the reaction proceeds for 96 h at 25 °C.[18] For the mixed acid method, 1 g of V_2AlC is added to a mixture of 12 mL of 48 wt % HF and 8 mL of 12 M HCl, and the reaction proceeds for 72 h at 50 °C. After etching is completed, the etchant mixture is diluted and transferred to 175 mL centrifuge tubes and centrifuged at 3500 rpm (2550 rcf) for 5 min. At this point, the *ml*-V_2CT_x, along with any remaining MAX phase, will be sedimented at the bottom of the tube, and a green supernatant, which is caused by vanadium ions in solution, is obtained (Figure 1b). It is important to note that the green supernatant observed at this stage is not MXene but is instead dissolved V from small intermetallics, residual metal, and nanosized MAX phase present in the precursor. Therefore, it should be decanted as waste. The multilayer powder was washed with DI water and centrifuged repeatedly until the pH of the supernatant was >5.5. The washing typically requires >1.5 L of deionized water per 1 g of etched MAX phase. The *ml*-

https://doi.org/10.1021/acs.chemmater.1c03508
Chem. Mater. 2022, 34, 499−509

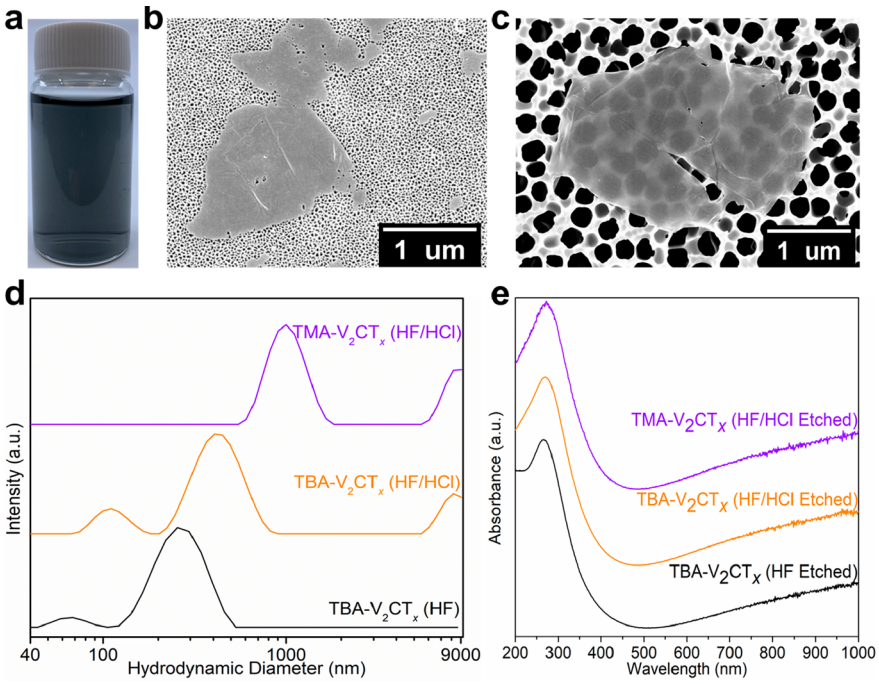

Figure 2. (a) Delaminated d-V_2CT_x solution (diluted). SEM images of TBA-V_2CT_x flakes from (b) HF etching and (c) HF/HCl etching on anodized aluminum oxide (AAO). (d) DLS measurements and (e) UV−vis measurements for TBA-V_2CT_x (HF and HF/HCl etch) and TMA-V_2CT_x.

V_2CT_x can be immediately delaminated (using the wet powder), dried for storage, or used and processed directly.

The ml-V_2CT_x powder exhibits a dark brown color compared to the gray MAX phase, which can be seen in Figure S2b,c, respectively. There is no apparent optical difference between the loose ml-V_2CT_x powders etched by HF or mixed acid etching, but when the multilayer powders are pressed into pellets, the mixed acid etch is brighter and more golden in color (Figure S2d,e). X-ray diffraction (XRD) patterns were collected at each stage of synthesis for both etching methods and are shown in Figure 1c. For the preparation of XRD samples, V_2CT_x was prepared simultaneously using both etching methods, followed by identical drying procedures. The multilayer powders were dried on a vacuum filter, followed by 24 h in a vacuum desiccator at RT. The powders were subsequently crushed into a fine powder and dried for an additional 48 h in the vacuum desiccator. A total of 200 mg of each multilayer powder was pressed into pellets at 50 MPa to orient the MXene powders along their basal planes. The shift of the (002) peak, from 13.44° in V_2AlC to 8.98° (mixed acid etch) and 9.22° (HF etch) for ml-V_2CT_x, is attributed to the successful removal of Al from V_2AlC and subsequent expansion of the $d_{(002)}$-spacing from 6.6 Å to 10 Å and 9.6 Å, respectively. The intensity of the MXene (002) peak relative to the MAX phase peaks is greater in the mixed acid etch, which is indicative of a more complete etching of the Al layers with higher yield of V_2CT_x MXene from the mixed acid etch. These XRD characteristics can be directly compared between the samples due to the identical precursor, processing conditions, and sample preparation. The SEM images in Figure 1d−f compare the layered structure of the V_2AlC MAX phase with the obtained ml-V_2CT_x. Both ml-V_2CT_x MXenes show an open and typical "accordion-like" structure (Figure 1e,f).

Delamination and Ion-Exchange Process. The ml-V_2CT_x powders are delaminated using tetrabutylammonium hydroxide (TBAOH; denoted TBA-V_2CT_x) or tetramethylammonium hydroxide (TMAOH; denoted TMA-V_2CT_x). For the best results (higher yield), delamination should be done immediately following etching and using the wet multilayer powder; however, it is also possible to delaminate vacuum-filter dried MXene powders. In the latter case, we suggest storing the dried ml-V_2CT_x powder under an inert atmosphere (i.e., inside the Ar-filled glovebox) and take it out when the delamination will be done.

The delamination protocols for TMAOH are as follows: ∼1 g of freshly etched ml-V_2CT_x powder (in the wet state) was added to 20 mL of a 5 wt % TMAOH solution in water, and the solution was stirred at 400 rpm at room temperature (25 °C) for 6 h. Alternatively, when dried ml-V_2CT_x is used for delamination, 200 mg of powder can be added to 10 mL of a 25 wt % TMAOH solution in water, and the solution should be stirred at 400 rpm at 35 °C for 6 h. Different delamination conditions are used because fresh (wet) multilayer MXene has preintercalated water between the layers, giving better ion mobility and intercalation,[34] enabling the process to occur more efficiently. When MXene multilayer powders are dried, the interlayer spacing and ion mobility between the layers decreases as the result of water deintercalation, leading to sluggish delamination kinetics and lower yield. Therefore, to achieve a higher yield (∼50%), we suggest using the freshly etched wet powders to prepare dispersions of d-V_2CT_x. Similar to TMAOH, the delamination protocols for TBAOH are ∼1 g of freshly etched ml-V_2CT_x powder added to 20 mL of a 5 wt % TBAOH solution in water, and the solution was stirred at 400 rpm at 25 °C for 6 h. Alternatively, 200 mg of dried ml-V_2CT_x was added to 10 mL of a 40 wt % TBAOH solution in water, and the solution was stirred at 400 rpm at 35 °C for 6 h.

After stirring in the delaminating agent, the intercalated multilayer powder is transferred to a centrifuge tube filled with DI water. The solution is centrifuged at 3500 rpm (2550 rcf)

https://doi.org/10.1021/acs.chemmater.1c03508
Chem. Mater. 2022, 34, 499−509

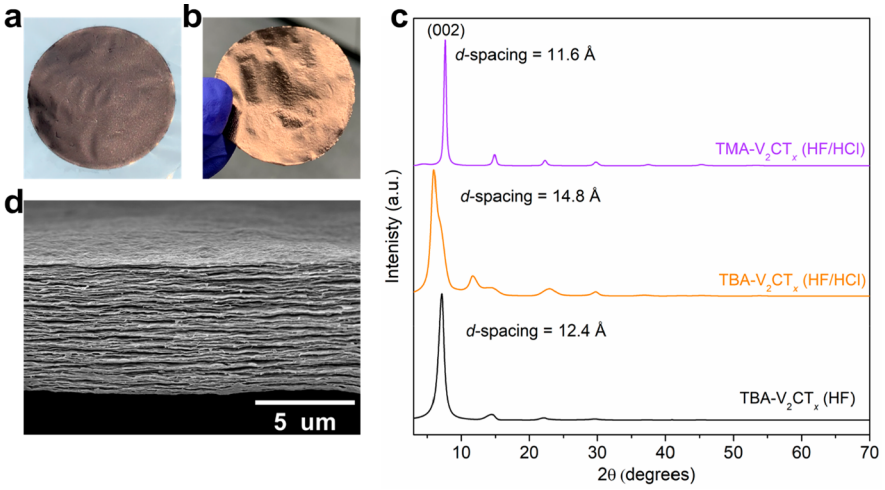

Figure 3. Optical image of vacuum filtered films made from (a) TBA-V_2CT_x (HF etched) and (b) TMA-V_2CT_x (HF/HCl etched). (c) SEM image of cross-section from the TMA-V_2CT_x vacuum filtered film. (d) XRD patterns of TBA-V_2CT_x (HF and HF/HCl) and TMA-V_2CT_x (HF/HCl etch).

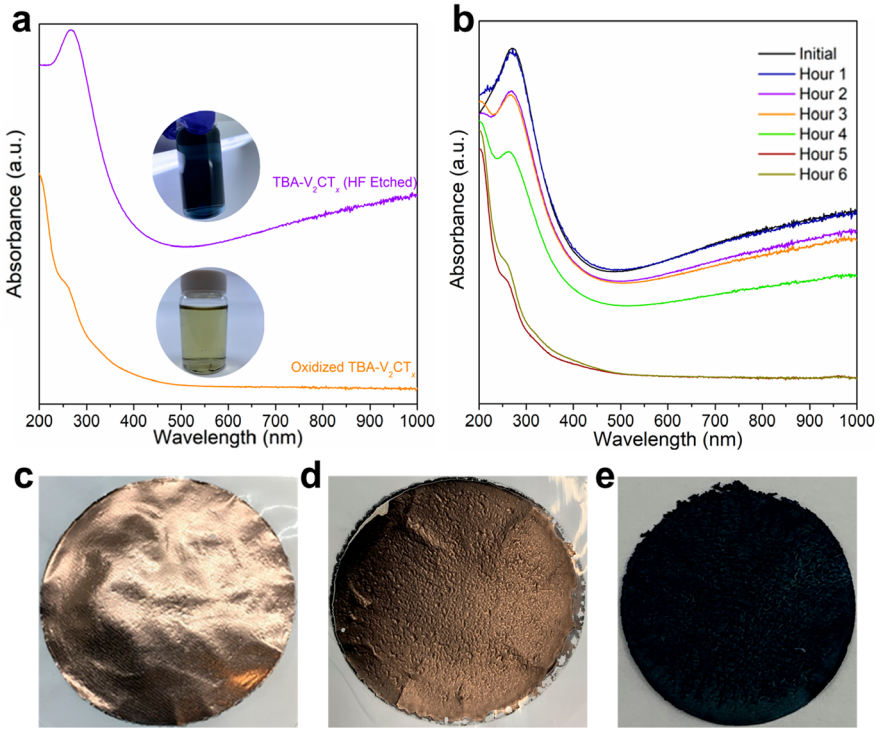

Figure 4. (a) UV−vis spectra of HF etched TBA-V_2CT_x and oxidized V_2CT_x solution. (b) UV−vis spectra of pristine HF/HCl TBA-V_2CT_x collected at 1 h intervals to show oxidation. TMA-V_2CT_x (HF/HCl etched) films (c) from pristine solution, (d) from 1 month old solution (stored in an argon filled vial), and (e) from pristine solution aged in air for 1 month after drying.

for 10 min, and the first supernatant is discarded. The sediment is dispersed in DI water and shaken by hand for 2 min before centrifuging at 2500 rpm (1300 rcf) for 10 min (higher centrifuge speeds result in lower concentration of *d*-V_2CT_x supernatant). It is crucial that the shaking process be performed for at least 2 min to ensure that the sediment is uniformly redispersed in fresh DI water. The second supernatant is once again discarded. After this stage, redispersion, hand shaking, and the 2500 rpm (1300 rcf) centrifugation is repeated with the supernatant being collected until the *d*-V_2CT_x concentration is low (when supernatant turns to a blue-green color or becomes transparent). This process will typically use ∼1.2 L of water for 1 g of MXene.

In Figure 2a, the dilute TBA-V_2CT_x solution (20 mL vial) is green-blue, while Figure 2b,c shows SEM images of the TBA-V_2CT_x flakes obtained from both HF and mixed acid etching methods drop-cast on an anodized aluminum oxide (AAO) membrane. Notably, depending on the type of the intercalant used, flakes with different physical properties are obtained; TMA^+ molecules are smaller than TBA^+ molecules, with hydrated ionic radii of 3.67 and 4.94 Å, respectively, so the corresponding flake size tends to be larger in the case of TMA^+.[35] This trend can be seen from the dynamic light

https://doi.org/10.1021/acs.chemmater.1c03508
Chem. Mater. 2022, 34, 499−509

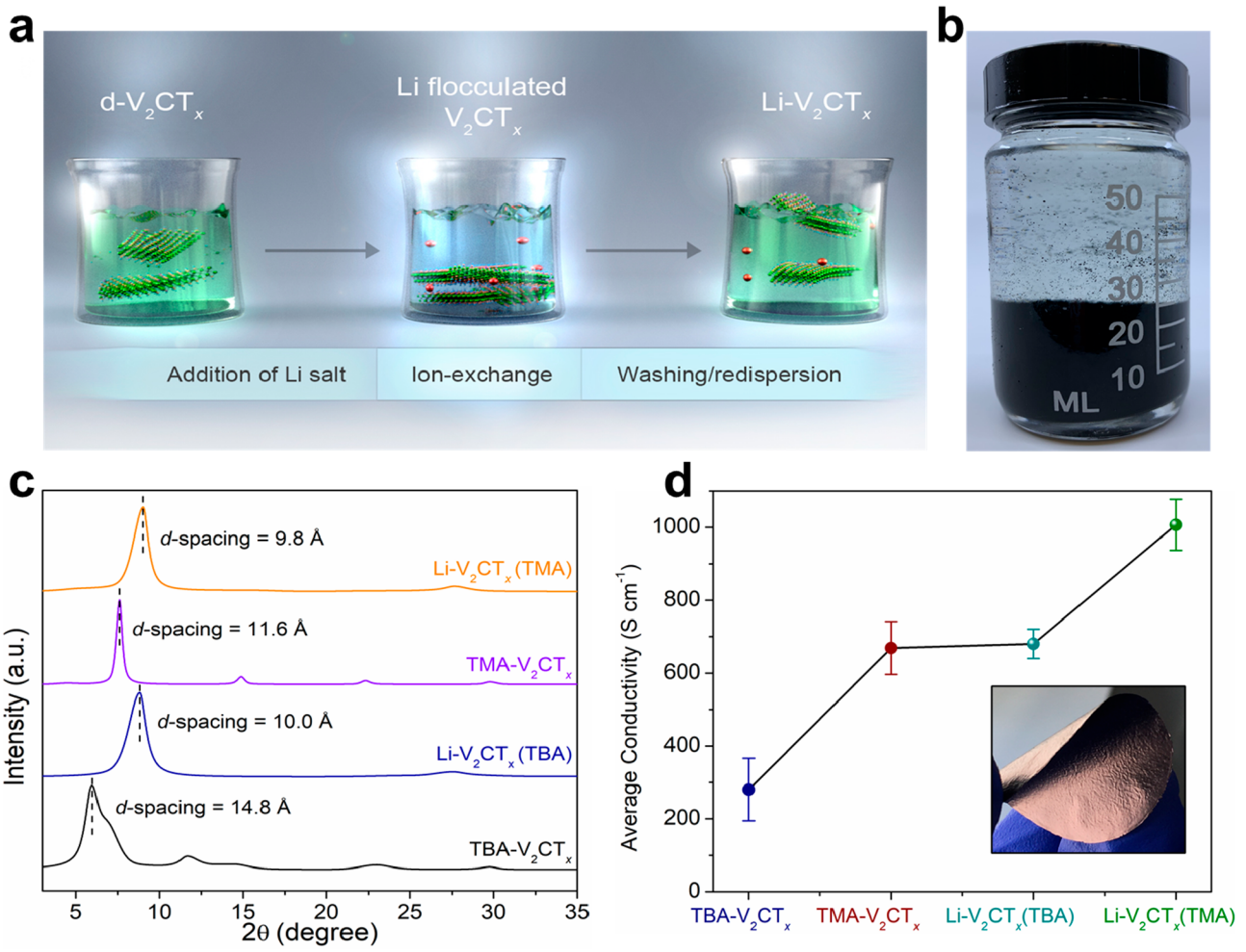

Figure 5. (a) Schematic of the ion-exchange procedure. (b) *d*-V_2CT_x solution flocculated using LiCl. (c) XRD patterns of TBA-V_2CT_x, TMA-V_2CT_x, and Li-V_2CT_x made from both samples. These samples were all vacuum-filtered films from the mixed acid synthesis (the TMA and TBA-V_2CT_x patterns are taken from Figure 3d). (d) Conductivity measurements from vacuum filtered V_2CT_x films with different interlayer ions (TBA^+, TMA^+, Li^+). Inset image of vacuum filtered Li-V_2CT_x (TBA) shown.

scattering (DLS) measurements shown in Figure 2d, and additionally, DLS reveals that the mixed acid etch results in larger flake sizes compared to HF etching. To study optical properties of the MXene colloids, UV−vis spectra were collected from TBA-V_2CT_x (HF and mixed acid) and TMA *d*-V_2CT_x (mixed acid) colloids and are shown in Figure 2e. The spectra for the HF etched sample shows a plateau in the low UV region (<250 nm), as seen in literature previously.[4] However, based on our current understanding, this peak indicates the degradation of *d*-V_2CT_x. The lack of such a peak or plateau in the mixed acid etched samples is an indicator that the mixed acid etch results in flakes with higher quality with minimal content of oxidized/degraded flakes immediately after synthesis. Binder free, freestanding flexible MXene films with a golden-brown color (shown in Figure 3a,b) were obtained by vacuum filtering (<20 mL) *d*-V_2CT_x dispersed in water on a Celgard 3501 (0.22 μm pore size, 40 mm diameter) membrane. The SEM image in Figure 3c shows the cross section of a TMA-V_2CT_x vacuum filtered film with a typical layered stack of individual MXene flakes. The corresponding XRD patterns of *d*-V_2CT_x films are shown in Figure 3d. The $d_{(002)}$-spacing of films prepared from TMA-V_2CT_x solutions (11.6 Å (2θ of 7.6°)) is smaller than that of TBA-V_2CT_x due to the smaller intercalant size. The TBA-V_2CT_x films from the HF etch and mixed acid etch show larger $d_{(002)}$-spacings of 12.4 Å (2θ of 7.1°) and 14.8 Å (2θ of 5.95°), respectively. This variation could be the result of flake size difference, remaining stacks of few-layer flakes in the HF sample, or an extra layer of water trapped in between the layers in the mixed acid sample.

As reported previously,[17,26] V_2CT_x is unstable once delaminated. The rapid degradation of *d*-V_2CT_x in water dispersions was studied using UV−vis spectroscopy. The complete oxidation of TBA-V_2CT_x (HF etched stored at 0.5 mg/mL) is shown in Figure 4a, with a color change from green-blue to yellow in the solution. The appearance of a second low-UV peak below 250 nm and a broad decrease in the intensity in the 500−1000 nm wavelength region further suggests the presence of vanadium oxide species in the oxidized solution.[22] Figure 4b shows the transformation of the spectra for dilute (0.1 mg/mL) TBA-V_2CT_x synthesized from the mixed acid etch (the same style graph is shown for the HF etch in Figure S4). The degradation begins immediately, with clear increases in the low UV region and reduction in the ∼275 nm V_2CT_x peak, making the HF etched sample completely unusable after 3 h and the mixed acid etch after 4 h. It is worth noting that a 1 h enhancement at such a dilute colloid may

https://doi.org/10.1021/acs.chemmater.1c03508
Chem. Mater. 2022, 34, 499−509

provide greater stability enhancements at higher concentrations.[29] This severe degradation is further shown in Figure 4c−e using films of TMA-V_2CT_x (mixed acid etch), vacuum filtered from fresh colloid, a one-month-old colloid (stored in argon filled vial in refrigerator), and a film prepared from a fresh colloid that was then left in the open air for one month. In all cases the films appear darker (compared to the brownish gold color for fresh films), but the oxidation in air was more detrimental as seen by the color and flexibility. This degradation can also be seen from the decrease in electrical conductivity of the films after oxidation. The film in Figure 4c exhibited a conductivity of 648 S cm $^{-1}$, while the films in Figure 4d,e had conductivities of 80 and 58 S cm^{-1}, respectively.

In order to overcome the rapid degradation and instability *d*-V_2CT_x, an ion-exchange process was used to replace the residual TBA^+ or TMA^+ with smaller alkali cations. It is worth noting that, in our experience, delamination with large organic TBA^+ or TMA^+ molecules is one of the culprits for defect formation in V_2CT_x flakes, an effect that may be more significant than harsh etching conditions. Therefore, development of etching and delamination procedures that eliminate the need for organic molecules and instead enable use of Li^+ (or other alkali ions) will be beneficial. Figure 5a schematically illustrates the ion exchange and flocculation processes used to remove residual organic intercalants, substitute them with Li cations, and redisperse *d*-V_2CT_x solutions that now contain Li residuals.

The ion exchange process removes adsorbed ions from the MXene surface (TBA^+, TMA^+) and replaces them with more desirable ions. This also results in tuning the MXene properties by changing their interlayer spacing and chemistry. An ion exchange process in multilayer $Ti_3C_2T_x$ MXene was previously demonstrated.[34] In conjunction with the ion exchange process, flocculation occurs due to the electrostatic adsorption of cations on the negatively charged MXene surface. Previous reports of the zeta potential (surface charge) of HF etched *d*-V_2CT_x showed an average zeta potential of −32.4, which is close to the limit of colloidal stability (−30 mV).[4] Using the mixed acid etch, average zeta potentials of −41.8 and −52.0 mV were achieved for TBA^+ and TMA^+ delaminated V_2CT_x, respectively, which is shown in Figure S5. With the addition of excess cations, flakes begin to crumple and restack in order to compensate for the charge of the positive ion on the negatively charged flakes, and the flocculated flakes precipitate out of solution. Flocculation of $Ti_3C_2T_x$ and V_2CT_x has been demonstrated using acids and bases, such as HCl and NaOH, as well as some alkali salts.[36−38]

In order to perform ion-exchange and flocculation on TBA- or TMA-V_2CT_x colloids, a saturated LiCl water dispersion (19.8 m) is used to exchange TMA^+/TBA^+ for Li^+. In a typical process, a 1:5 volume ratio of 19.8 m LiCl solution to MXene solution (concentration of ∼0.5−1.0 mg/mL) was used. It is important to perform this process immediately after fresh *d*-V_2CT_x solutions are prepared to avoid degradation. After the sample has been flocculated, it should be left to naturally settle before any further handling. After the flocs have completely settled, if the sample is going to be kept for long-term storage (more than 2 weeks), the supernatant, which contains TMA^+/TBA^+, H_2O, and excess Li^+, should be removed and replaced with 19.8 m LiCl solution. This can be accomplished using a pipet to remove the clear supernatant over the flocculated MXene, followed by replacing the same volume with 19.8 m LiCl. This maximizes the LiCl:water ratio, minimizing hydrolysis.[39] Centrifugation may yield the same result, but there may be a difference in the structure and stacking of the centrifuged flocs, which may affect redispersibility. This process allows *d*-V_2CT_x to be kept in a wet flocculated state (in a fridge) for storage until use. The flocculated V_2CT_x can be redispersed by washing with DI water and removal of excess Li ions (similar to washing after conventional intercalation/delamination). In short, the wet precipitates are transferred to centrifuge tubes and centrifuged at 3500 rpm (2550 rcf) for 10 min in order to ensure sedimentation of the flocculated MXene. The supernatant is decanted, and the washing process is continued by redispersing the precipitates in DI water, followed by hand shaking for 2 min between cycles. This is typically repeated 3−5 times, using ∼750 mL of DI water for 1 g of V_2CT_x. Afterward, the V_2CT_x flakes start to redisperse in water (supernatant becomes green/blue), and the supernatant can be collected. The obtained solutions are labeled as Li-V_2CT_x. The flocculated V_2CT_x solutions are shown in Figure 5b. For comparison, Li-V_2CT_x was prepared from TBA-V_2CT_x (HF and mixed acid etch) as well as TMA-V_2CT_x (mixed acid etch), and XRD analysis was performed on the vacuum filtered films. There is a clear and distinct shift in the position of (00*l*) basal planes of V_2CT_x toward higher Bragg angles (smaller *d*-spacing) after ion-exchange, which indicates substitution of the majority of large TBA^+/TMA^+ ions with smaller Li^+ in the interlayer space. Moreover, there is a negligible difference in the $d_{(002)}$-spacing (0.2 Å) of the Li-V_2CT_x films obtained from TMA or TBA-V_2CT_x solutions (Figure 5c), which indicates that the ion exchange process can be done efficiently on both of these intercalants. The removal of residual TBA^+ and TMA^+ during the ion-exchange process was further investigated by using thermogravimetric analysis (TGA) as shown in Figure S6a−e. Both TBA and TMA delaminated V_2CT_x samples showed a notable weight loss at ∼400 °C (Figure S6b,c), which is attributed to the decomposition and removal of residual intercalants (TBA^+ or TMA^+).[40] However, similar to *ml*-V_2CT_x, the TGA analysis of Li ion-exchanged V_2CT_x samples did not show a weight loss peak in this temperature range, suggesting removal of residual TBA and TMA intercalants in these samples and high efficiency of the ion-exchange process.

In addition, compared to the previous report on ion-exchanged Li-V_2CT_x vacuum filtered films, our optimized process results in a more efficient removal of residual TBA^+ or TMA^+.[19] This can be seen from the obtained *d*-spacing values, where our Li-V_2CT_x films (prepared from TBA delaminated solutions) show a $d_{(002)}$ of ∼10.0 Å, whereas a value of 12.2 Å was reported in the previous work.[19] Figure 5d shows the conductivities of the V_2CT_x films obtained from vacuum filtration of different V_2CT_x solutions with different intercalants. The Li-V_2CT_x freestanding films exhibit electrical conductivity >1000 S cm^{-1} without annealing, roughly twice those of previous reports.[21] The observed differences in the electrical conductivities of TBA or TMA-V_2CT_x and their corresponding Li-V_2CT_x films are likely due to differences in V_2CT_x flake size and quality. Larger V_2CT_x flake sizes in TMA intercalated films generally result in higher electrical conductivity compared to TBA intercalated films (a similar relationship has been reported for $Ti_3C_2T_x$).[41] The decrease in the interlayer spacing of all Li-V_2CT_x films further facilitates interflake electron transport, and therefore, these films show the highest electrical conductivity. Li-V_2CT_x obtained from

https://doi.org/10.1021/acs.chemmater.1c03508
Chem. Mater. 2022, 34, 499−509

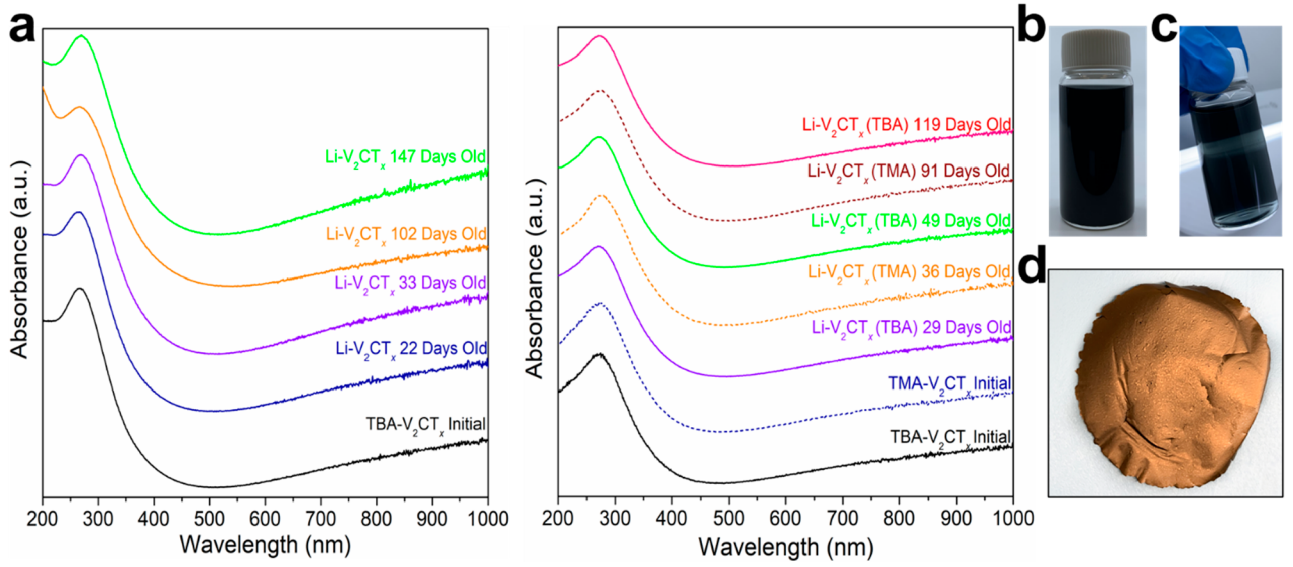

Figure 6. UV−vis spectra of (a) HF etched V_2CT_x and HF/HCl etched V_2CT_x kept flocculated over different periods of time. (b) Concentrated and (c) dilute Li-V_2CT_x solution redispersed after 147 days. (d) Vacuum filtered Li-V_2CT_x film made from 147 day old solution.

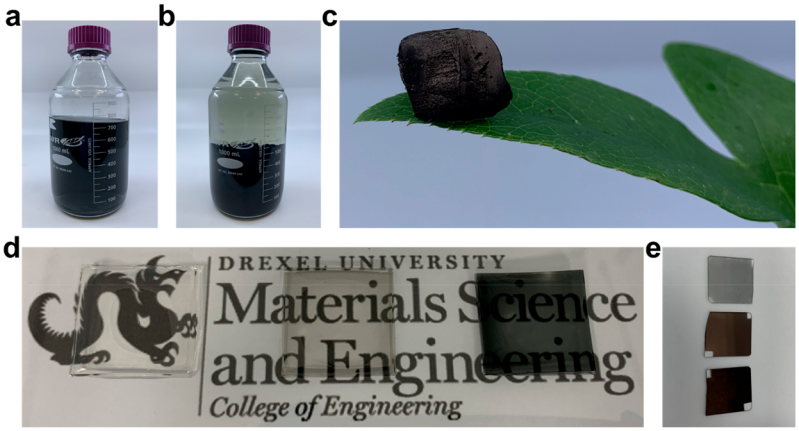

Figure 7. Digital photographs of (a) a large volume of TMA-V_2CT_x solution, (b) a flocculated Li-V_2CT_x solution, (c) a Li-V_2CT_x aerogel, (d) Li-V_2CT_x/PVA hydrogels of increasing MXene concentration (logo credited to Drexel University, College of Engineering), and (e) a Li-V_2CT_x solution spray coated on glass with increasing thickness.

TMA-V_2CT_x solution shows a slightly higher conductivity as the result of its larger flake size. Additional factors that may influence the conductivity include the cations and water present in the interlayer of the V_2CT_x, but these factors are complex and not currently well understood. The ion exchange and flocculation process can be performed with other ions, as Na^+ and Mg^{2+} have been demonstrated previously.[19] However, it is unlcear if the stability increase will be as significant due to the lower molarity of other saturated salts compared to 19.8 m LiCl. We speculate that monovalent, high molarity salts such as 30 m potassium acetate could be used similarly.

The stability of the redispersed Li-V_2CT_x solutions was studied via UV−vis as shown in Figure 6a. TBA-V_2CT_x (HF etched) was kept in the flocculated state and redispersed after 33 and 147 days. Even after 147 days, the increase in the low UV region peak was minor and within the limits of what has been considered pristine *d*-V_2CT_x solutions in previous works.[4] This 147 day old Li-V_2CT_x solution showed no visible signs of degradation, as seen in Figure 6b,c. The solution was subsequently vacuum filtered into a film that showed bright golden-brown color and good flexibility (Figure 6d) in contrast to the TMA-V_2CT_x (Figure 4d), which was prepared only after 30 days of storage. It is worth noting that the 102 day old sample had higher degradation than the 147 day old sample, which we assume is due to variation in the original samples. The same UV−vis experiment was performed on Li^+ exchanged TMA and TBA-V_2CT_x (mixed acid etched) solutions, and the sample stability was checked at various times. Both mixed acid etched samples show no change in the UV−vis spectra, indicating no degradation over time. This is in agreement with our visual observations where the diluted redispersed Li-V_2CT_x solution showed no distinctive color change after 119 days and preserved its greenish blue color.

Solution Processing of Li-V_2CT_x. The improved quality and long-term stability of Li-V_2CT_x enables processing of these solutions in a variety of different ways, similar to $Ti_3C_2T_x$. As a proof of concept and for practicality and useability of the produced V_2CT_x solutions, we demonstrate a few common processing techniques to fabricate V_2CT_x materials with different forms and structures. Figure 7a,b shows a 750 mL

https://doi.org/10.1021/acs.chemmater.1c03508
Chem. Mater. 2022, 34, 499−509

bottle of TMA-V_2CT_x solution and the flocculated Li-V_2CT_x, respectively. After redispersing, the Li-V_2CT_x solution was freeze-dried into an aerogel (Figure 7c), which can be used for EMI shielding, adsorption, and electrochemical applications. The prepared Li-V_2CT_x solutions can be used to prepare hydrogels as well. Hydrogels of varying transparency were prepared using mixtures of Li-V_2CT_x and PVA solutions in different ratios. The hydrogels (Figure 7d) showed distinct optical properties and mechanical flexibility. They can be used in biomedical applications like physiological sensors and bioelectronic interfaces, as well as electrochemical applications related to flexible, solid-state energy storage. Moreover, The V_2CT_x solutions can also be processed using spray coating. Transparent thin film V_2CT_x coatings were prepared by spray coating the Li-V_2CT_x solution with varying thicknesses onto glass slides (Figure 7e). This is a relatively low-cost, simple method to generate transparent, conductive electrodes for electrochemical and optoelectronic applications. These examples demonstrate that the improved stability and properties of V_2CT_x MXene obtained through protocols and methods explained in this paper can open new pathways for practical use of V_2CT_x in a wide range of new applications.

Characterization Techniques and Procedure. A Zeiss Supra 50VP SEM was used for imaging of the V_2AlC powder, multilayered and delaminated V_2CT_x, and vacuum filtered films. A Rigaku Smart Lab and powder diffractometer with a Cu K_α target was used to collect XRD patterns from samples. MAX phase samples were scanned from 3 to 90° 2θ, while MXene samples were scanned from 3 to 70° 2θ. A current of 15 mA and a voltage of 40 kV were used with a step size of 0.02° 2θ and a duration time of 0.4 s. An Evolution 201 UV−vis spectrophotometer (Thermo Scientific, MA, U.S.A.) with a 10 mm optical path length quartz cuvette was used for analyses of optical properties. Spectra were collected from 200 to 1000 nm. Electrical conductivity of vacuum filtered V_2CT_x films and pressed multilayer V_2CT_x pellets were measured using a four-point probe conductivity measurement technique equipped with a 1 mm probe (Jandel Engineering Ltd., Bedforshire, U.K.). The measured sheet resistance was converted to conductivity (S cm^{-1}) by factoring in the calculated thicknesses from either the SEM or the micrometer. Flake size and zeta potential of solutions were estimated using a Malvern Panalytical Zetasizer Nano ZS in a folded capillary disposable cuvette. Five measurements were recorded in both cases, with the average being recorded.

SUMMARY

In this paper, we show how to overcome stability limitations when working with V_2CT_x, which is known as one of the least stable MXenes. The viability of using a mixed acid etchant for the synthesis of this MXene was shown. We developed an efficient and robust ion-exchange protocol that increases its chemical stability, both in wet and dry forms. Most important, the stability of delaminated V_2CT_x MXene in aqueous solutions increased from a few hours to several months, opening new horizons for applications of this material having many attractive properties. This ion exchange process enables tuning of the interlayer space, resulting in an increased electrical conductivity of V_2CT_x freestanding films above all the values reported in the literature. We have demonstrated and discussed improved etching, delamination, and storage approaches and protocols for V_2CT_x. Therefore, this work can be looked at as a comprehensive guideline for the synthesis of chemically stable V_2CT_x MXene solutions and films with improved properties.

ASSOCIATED CONTENT

Supporting Information

The Supporting Information is available free of charge at https://pubs.acs.org/doi/10.1021/acs.chemmater.1c03508.

Schematic of the etching parametric study, optical images of etching setup and MAX/MXene samples, characterization of V_2CT_x using XRD, UV−vis, SEM, zeta potential, and TGA, nomenclature guidelines, and chemical suppliers list (PDF)

AUTHOR INFORMATION

Corresponding Author

Yury Gogotsi − *A.J. Drexel Nanomaterials Institute and Department of Materials Science and Engineering, Drexel University, Philadelphia, Pennsylvania 19104, United States;* orcid.org/0000-0001-9423-4032; Email: gogotsi@drexel.edu

Authors

Kyle Matthews − *A.J. Drexel Nanomaterials Institute and Department of Materials Science and Engineering, Drexel University, Philadelphia, Pennsylvania 19104, United States*

Teng Zhang − *A.J. Drexel Nanomaterials Institute and Department of Materials Science and Engineering, Drexel University, Philadelphia, Pennsylvania 19104, United States*

Christopher E. Shuck − *A.J. Drexel Nanomaterials Institute and Department of Materials Science and Engineering, Drexel University, Philadelphia, Pennsylvania 19104, United States;* orcid.org/0000-0002-1274-8484

Armin VahidMohammadi − *A.J. Drexel Nanomaterials Institute and Department of Materials Science and Engineering, Drexel University, Philadelphia, Pennsylvania 19104, United States;* orcid.org/0000-0002-6284-7560

Complete contact information is available at: https://pubs.acs.org/10.1021/acs.chemmater.1c03508

Notes

The authors declare no competing financial interest.

ACKNOWLEDGMENTS

The authors would like to acknowledge Dr. Tyler Mathis for discussion about MAX and MXene synthesis protocols and his assistance with SEM analysis, Mark Anayee for training and assistance with TGA analysis, and Natalia Noriega for manufacturing MXene/PVA hydrogels. This work was supported by the Fluid Interface Reactions, Structures, and Transport (FIRST) Center, an Energy Frontier Research Center funded by the U.S. Department of Energy, Office of Science, and Office of Basic Energy Sciences for MXene electrochemistry research.

REFERENCES

(1) Naguib, M.; Kurtoglu, M.; Presser, V.; Lu, J.; Niu, J.; Heon, M.; Hultman, L.; Gogotsi, Y.; Barsoum, M. W. Two-Dimensional Nanocrystals Produced by Exfoliation of Ti_3AlC_2. *Adv. Mater.* **2011**, *23* (37), 4248−4253.

(2) Khazaei, M.; Ranjbar, A.; Arai, M.; Sasaki, T.; Yunoki, S. Electronic Properties and Applications of MXenes: A Theoretical Review. *J. Mater. Chem. C* **2017**, *5* (10), 2488−2503.

(3) Lipatov, A.; Lu, H.; Alhabeb, M.; Anasori, B.; Gruverman, A.; Gogotsi, Y.; Sinitskii, A. Elastic Properties of 2D $Ti_3C_2T_x$ MXene Monolayers and Bilayers. *Sci. Adv.* **2018**, *4* (6), No. eaat0491.
(4) Maleski, K.; Shuck, C. E.; Fafarman, A. T.; Gogotsi, Y. The Broad Chromatic Range of Two-Dimensional Transition Metal Carbides. *Adv. Opt. Mater.* **2021**, *9* (4), 2001563.
(5) Anasori, B.; Lukatskaya, M. R.; Gogotsi, Y. 2D Metal Carbides and Nitrides (MXenes) for Energy Storage. *Nat. Rev. Mater.* **2017**, *2* (2), 16098.
(6) Shahzad, F.; Alhabeb, M.; Hatter, C. B.; Anasori, B.; Man Hong, S.; Koo, C. M.; Gogotsi, Y. Electromagnetic Interference Shielding with 2D Transition Metal Carbides (MXenes). *Science* **2016**, *353* (6304), 1137−1140.
(7) Iqbal, A.; Shahzad, F.; Hantanasirisakul, K.; Kim, M. K.; Kwon, J.; Hong, J.; Kim, H.; Kim, D.; Gogotsi, Y.; Koo, C. M. Anomalous Absorption of Electromagnetic Waves by 2D Transition Metal Carbonitride Ti_3CNT_x (MXene). *Science* **2020**, *369* (6502), 446−450.
(8) Lee, E.; Vahidmohammadi, A.; Prorok, B. C.; Yoon, Y. S.; Beidaghi, M.; Kim, D. J. Room Temperature Gas Sensing of Two-Dimensional Titanium Carbide (MXene). *ACS Appl. Mater. Interfaces* **2017**, *9* (42), 37184−37190.
(9) Kim, S. J.; Koh, H. J.; Ren, C. E.; Kwon, O.; Maleski, K.; Cho, S. Y.; Anasori, B.; Kim, C. K.; Choi, Y. K.; Kim, J.; Gogotsi, Y.; Jung, H. T. Metallic $Ti_3C_2T_x$ MXene Gas Sensors with Ultrahigh Signal-to-Noise Ratio. *ACS Nano* **2018**, *12* (2), 986−993.
(10) Lyu, B.; Kim, M.; Jing, H.; Kang, J.; Qian, C.; Lee, S.; Cho, J. H. Large-Area MXene Electrode Array for Flexible Electronics. *ACS Nano* **2019**, *13* (10), 11392−11400.
(11) Melianas, A.; Kang, M.-A.; VahidMohammadi, A.; Quill, T. J.; Tian, W.; Gogotsi, Y.; Salleo, A.; Hamedi, M. M. High-Speed Ionic Synaptic Memory Based on 2D Titanium Carbide MXene. *Adv. Funct. Mater.* **2021**, 2109970.
(12) Meng, F.; Seredych, M.; Chen, C.; Gura, V.; Mikhalovsky, S.; Sandeman, S.; Ingavle, G.; Ozulumba, T.; Miao, L.; Anasori, B.; Gogotsi, Y. MXene Sorbents for Removal of Urea from Dialysate: A Step toward the Wearable Artificial Kidney. *ACS Nano* **2018**, *12*, 10518−10528.
(13) Mojtabavi, M.; Vahidmohammadi, A.; Liang, W.; Beidaghi, M.; Wanunu, M. Single-Molecule Sensing Using Nanopores in Two-Dimensional Transition Metal Carbide (MXene) Membranes. *ACS Nano* **2019**, *13* (3), 3042−3053.
(14) Lin, H.; Wang, X.; Yu, L.; Chen, Y.; Shi, J. Two-Dimensional Ultrathin MXene Ceramic Nanosheets for Photothermal Conversion. *Nano Lett.* **2017**, *17* (1), 384−391.
(15) VahidMohammadi, A.; Rosen, J.; Gogotsi, Y. The World of Two-Dimensional Carbides and Nitrides (MXenes). *Science (80-).* **2021**, *372* (6547), No. eabf1581.
(16) *2D Metal Carbides and Nitrides (MXenes): Structure, Properties and Applications*; Anasori, B., Gogotsi, Y., Eds.; Springer International Publishing: Cham, 2019; DOI: 10.1007/978-3-030-19026-2.
(17) Vahidmohammadi, A.; Hadjikhani, A.; Shahbazmohamadi, S.; Beidaghi, M. Two-Dimensional Vanadium Carbide (MXene) as a High-Capacity Cathode Material for Rechargeable Aluminum Batteries. *ACS Nano* **2017**, *11* (11), 11135−11144.
(18) Naguib, M.; Halim, J.; Lu, J.; Cook, K. M.; Hultman, L.; Gogotsi, Y.; Barsoum, M. W. New Two-Dimensional Niobium and Vanadium Carbides as Promising Materials for Li-Ion Batteries. *J. Am. Chem. Soc.* **2013**, *135* (43), 15966−15969.
(19) VahidMohammadi, A.; Mojtabavi, M.; Caffrey, N. M.; Wanunu, M.; Beidaghi, M. Assembling 2D MXenes into Highly Stable Pseudocapacitive Electrodes with High Power and Energy Densities. *Adv. Mater.* **2019**, *31* (8), 1806931.
(20) Lee, E.; VahidMohammadi, A.; Yoon, Y. S.; Beidaghi, M.; Kim, D.-J. Two-Dimensional Vanadium Carbide MXene for Gas Sensors with Ultrahigh Sensitivity Toward Nonpolar Gases. *ACS Sensors* **2019**, *4* (6), 1603−1611.
(21) Ying, G.; Kota, S.; Dillon, A. D.; Fafarman, A. T.; Barsoum, M. W. Conductive Transparent V_2CT_x (MXene) Films. *FlatChem.* **2018**, *8* (March), 25−30.
(22) Huang, D.; Xie, Y.; Lu, D.; Wang, Z.; Wang, J.; Yu, H.; Zhang, H. Demonstration of a White Laser with V_2C MXene-Based Quantum Dots. *Adv. Mater.* **2019**, *31* (24), 1901117.
(23) Champagne, A.; Shi, L.; Ouisse, T.; Hackens, B.; Charlier, J.-C. C. Electronic and Vibrational Properties of V_2C-Based MXenes: From Experiments to First-Principles Modeling. *Phys. Rev. B: Condens. Matter Mater. Phys.* **2018**, *97* (11), 115439.
(24) Urbankowski, P.; Anasori, B.; Hantanasirisakul, K.; Yang, L.; Zhang, L.; Haines, B.; May, S. J.; Billinge, S. J. L.; Gogotsi, Y. 2D Molybdenum and Vanadium Nitrides Synthesized by Ammoniation of 2D Transition Metal Carbides (MXenes). *Nanoscale* **2017**, *9*, 17722.
(25) Thakur, R.; Vahidmohammadi, A.; Moncada, J.; Adams, W. R.; Chi, M.; Tatarchuk, B.; Beidaghi, M.; Carrero, C. A. Insights into the Thermal and Chemical Stability of Multilayered V_2CT_x MXene. *Nanoscale* **2019**, *11* (22), 10716−10726.
(26) Naguib, M.; Unocic, R. R.; Armstrong, B. L.; Nanda, J. Large-Scale Delamination of Multi-Layers Transition Metal Carbides and Carbonitrides "MXenes". *Dalt. Trans.* **2015**, *44* (20), 9353−9358.
(27) Alhabeb, M.; Maleski, K.; Anasori, B.; Lelyukh, P.; Clark, L.; Sin, S.; Gogotsi, Y. Guidelines for Synthesis and Processing of Two-Dimensional Titanium Carbide ($Ti_3C_2T_x$ MXene). *Chem. Mater.* **2017**, *29* (18), 7633−7644.
(28) Natu, V.; Hart, J. L.; Sokol, M.; Chiang, H.; Taheri, M. L.; Barsoum, M. W. Edge Capping of 2D-MXene Sheets with Polyanionic Salts To Mitigate Oxidation in Aqueous Colloidal Suspensions. *Angew. Chem., Int. Ed.* **2019**, *58* (36), 12655−12660.
(29) Zhao, X.; Vashisth, A.; Blivin, J. W.; Tan, Z.; Holta, D. E.; Kotasthane, V.; Shah, S. A.; Habib, T.; Liu, S.; Lutkenhaus, J. L.; Radovic, M.; Green, M. J. PH, Nanosheet Concentration, and Antioxidant Affect the Oxidation of $Ti_3C_2T_x$ and Ti_2CT_x MXene Dispersions. *Adv. Mater. Interfaces* **2020**, *7* (20), 2000845.
(30) Mathis, T. S.; Maleski, K.; Goad, A.; Sarycheva, A.; Anayee, M.; Foucher, A. C.; Hantanasirisakul, K.; Shuck, C. E.; Stach, E. A.; Gogotsi, Y. Modified MAX Phase Synthesis for Environmentally Stable and Highly Conductive Ti_3C_2 MXene. *ACS Nano* **2021**, *15* (4), 6420−6429.
(31) Sang, X.; Xie, Y.; Lin, M. W.; Alhabeb, M.; Van Aken, K. L.; Gogotsi, Y.; Kent, P. R. C.; Xiao, K.; Unocic, R. R. Atomic Defects in Monolayer Titanium Carbide ($Ti_3C_2T_x$) MXene. *ACS Nano* **2016**, *10* (10), 9193−9200.
(32) Shuck, C. E.; Ventura-Martinez, K.; Goad, A.; Uzun, S.; Shekhirev, M.; Gogotsi, Y. Safe Synthesis of MAX and MXene: Guidelines to Reduce Risk During Synthesis. *J. Chem. Health Saf.* **2021**, *28* (5), 326−338.
(33) Sarycheva, A.; Polemi, A.; Liu, Y.; Dandekar, K.; Anasori, B.; Gogotsi, Y. 2D Titanium Carbide (MXene) for Wireless Communication. *Sci. Adv.* **2018**, *4* (9), No. eaau0920.
(34) Ghidiu, M.; Halim, J.; Kota, S.; Bish, D.; Gogotsi, Y.; Barsoum, M. W. Ion-Exchange and Cation Solvation Reactions in Ti_3C_2 MXene. *Chem. Mater.* **2016**, *28* (10), 3507−3514.
(35) Gao, H.; Li, J.; Lian, K. Alkaline Quaternary Ammonium Hydroxides and Their Polymer Electrolytes for Electrochemical Capacitors. *RSC Adv.* **2014**, *4* (41), 21332−21339.
(36) Zhao, D.; Clites, M.; Ying, G.; Kota, S.; Wang, J.; Natu, V.; Wang, X.; Pomerantseva, E.; Cao, M.; Barsoum, M. W. Alkali-Induced Crumpling of $Ti_3C_2T_x$ (MXene) to Form 3D Porous Networks for Sodium Ion Storage. *Chem. Commun.* **2018**, *54* (36), 4533−4536.
(37) Natu, V.; Clites, M.; Pomerantseva, E.; Barsoum, M. W. Mesoporous MXene Powders Synthesized by Acid Induced Crumpling and Their Use as Na-Ion Battery Anodes. *Mater. Res. Lett.* **2018**, *6* (4), 230−235.
(38) Deng, Y.; Shang, T.; Wu, Z.; Tao, Y.; Luo, C.; Liang, J.; Han, D.; Lyu, R.; Qi, C.; Lv, W.; Kang, F.; Yang, Q. H. Fast Gelation of $Ti_3C_2T_x$ MXene Initiated by Metal Ions. *Adv. Mater.* **2019**, *31* (43), 1902432.

(39) Huang, S.; Mochalin, V. N. Hydrolysis of 2D Transition-Metal Carbides (MXenes) in Colloidal Solutions. *Inorg. Chem.* **2019**, *58* (3), 1958−1966.
(40) Seredych, M.; Shuck, C. E.; Pinto, D.; Alhabeb, M.; Precetti, E.; Deysher, G.; Anasori, B.; Kurra, N.; Gogotsi, Y. High-Temperature Behavior and Surface Chemistry of Carbide MXenes Studied by Thermal Analysis. *Chem. Mater.* **2019**, *31* (9), 3324−3332.
(41) Maleski, K.; Ren, C. E.; Zhao, M. Q.; Anasori, B.; Gogotsi, Y. Size-Dependent Physical and Electrochemical Properties of Two-Dimensional MXene Flakes. *ACS Appl. Mater. Interfaces* **2018**, *10* (29), 24491−24498.

https://doi.org/10.1021/acs.chemmater.1c03508
Chem. Mater. 2022, 34, 499−509